Published in Cell Motility and the Cytoskeleton 65, issue 10, 769-784, 2008
which should be used for any reference to this work

The Knock-Out of ARP3a Gene Affects F-Actin Cytoskeleton Organization Altering Cellular Tip Growth, Morphology and Development in Moss Physcomitrella Patens

Andrija Finka,* Younousse Saidi, Pierre Goloubinoff, Jean-Marc Neuhaus, Jean-Pierre Zrÿd, and Didier G. Schaefer

Department of Plant Molecular Biology, University of Lausanne, Lausanne, Switzerland

The seven subunit Arp2/3 complex is a highly conserved nucleation factor of actin microfilaments. We have isolated the genomic sequence encoding a putative Arp3a protein of the moss *Physcomitrella patens*. The disruption of this ARP3A gene by allele replacement has generated loss-of-function mutants displaying a complex developmental phenotype. The loss-of function of ARP3A gene results in shortened, almost cubic chloronemal cells displaying affected tip growth and lacking differentiation to caulonemal cells. In moss *arp3a* mutants, buds differentiate directly from chloronemata to form stunted leafy shoots having differentiated leaves similar to wild type. Yet, rhizoids never differentiate from stem epidermal cells. To characterize the F-actin organization in the *arp3a*-mutated cells, we disrupted ARP3A gene in the previously described HGT1 strain expressing conditionally the GFP-talin marker. In vivo observation of the F-actin cytoskeleton during *P. patens* development demonstrated that loss-of-function of Arp3a is associated with the disappearance of specific F-actin cortical structures associated with the establishment of localized cellular growth domains. Finally, we show that constitutive expression of the *P. patens* Arp3a and its *Arabidopsis thaliana* orthologs efficiently complement the mutated phenotype indicating a high degree of evolutionary conservation of the Arp3 function in land plants.

Key words: Arp2/3; actin cytoskeleton; GFP-talin; moss; *Physcomitrella patens*

Contract grant sponsor: Swiss National Science Foundation; Contract grant numbers: 31-51853.97, 3100A0-109290.

Pierre Goloubinoff and Jean-Pierre Zrÿd present address is Département de Biologie Moléculaire Végétale, Université de Lausanne, CH-1015 Lausanne, Switzerland.

Younousse Saidi's present address is Department of Biology, University of York, York YO10 5DD, United Kingdom.

Jean-Marc Neuhaus and Didier G. Schaefer's present address is Laboratoire de Biologie Moléculaire et Cellulaire, Institut de Botanique, Université de Neuchâtel, rue Emile-Argand 11, CH-2007 Neuchâtel, Switzerland.

*Correspondence to: Andrija Finka, Département de Biologie Moléculaire Végétale, Université de Lausanne, CH-1015 Lausanne, Switzerland.
E-mail: andrija.finka@unil.ch

INTRODUCTION

In eukaryotic cells, the actin cytoskeleton is directly involved in both cell growth and cytokinesis. Actin dynamic refers to the processes that regulate the balance between the formation and the dissociation of filamentous actin structures (F-actin) and a cellular pool of monomeric globular actin. These processes are mediated by a number of actin binding protein (ABP) complexes with distinct and/or overlapping functions: for example profilin controls the cellular pool of monomeric actin, actin depolymerising factors (ADF) are involved in the depolymerization of actin filaments while formins promote actin nucleation and fimbrin the association of actin filaments to form larger structures [Dos Remedios et al., 2003].

The Arp2/3 seven-subunit complex, along with formins, represents the two separate nucleation factors of actin moieties [Chang and Peter, 2002]. The complex promotes actin polymerization and nucleates novel filaments at the side of already existing ones in response to the activation of nucleation promoting factors of the WAVE/Scar complex [Szymanski, 2005]. This complex is formed of two actin-related proteins (Arp2 and Arp3) and five protein subunits (Arpc1 to Arpc5) that are conserved in eukaryotes. Its implication in the generation of networks of actin microfilaments at localized cellular sites is well documented in animal, yeast and plant cells. Its proper functioning is clearly important for some organisms, but it is not essential for all eukaryotes. In yeasts, *S. cerevisiae* and *S. pombe*, disruption of genes that encode subunits of the Arp2/3 complex causes severe growth defects or lethality consecutive to a defect in endocytotic vesicle dynamics [Lees-Miller et al., 1992; Balasubramanian et al., 1996; Winter et al., 1997; Morrell et al., 1999; Winter et al., 1999]. In fruit fly, the inactivation of ARP2/3 gene functions leads to lethality before adulthood [Hudson and Cooley, 2002; Zallen et al., 2002]. RNA interference (RNAi)-mediated knockdown of Arp2/3 subunits in *C. elegans* and human HeLa cells is lethal [Harborth et al., 2001; Sawa et al., 2003]. In mouse, *arp3* transposon-inserted mutants developed only to the blastocyst stage [Yae et al., 2006]. These dramatic phenotypes are most likely associated with defects in membrane protrusion and associated mobility processes essential during the early stages of animal development.

In contrast, deficiency of the Arp2/3 complex is perfectly viable in plants [Deeks and Hussey, 2005]. In *Arabidopsis thaliana*, loss of function phenotypes linked to mutations in subunits of the Arp2/3 and the Scar/Wave complex fall into the distorted group of mutants [Basu et al., 2005; Mathur, 2005; Le et al., 2006]. These mutants are mainly affected in epidermal cell expansion: they develop distorted leaf trichomes and display reduced expansion of leaf pavement and stem hypocotyl epidermal cells. Inhibition of tip growth in root hairs has been observed, but growth of pollen tube is not seriously affected. These growth defects were reproducibly associated with partial disorganization of the actin cytoskeleton but the specific F-actin population lost in *arp2/3* mutants is still a matter of debate [Deeks and Hussey, 2005; Mathur, 2005].

The moss *Physcomitrella patens* is emerging as a complementary model system to *Arabidopsis* and rice for evolutionary genetic approaches in plants due to its unique capacity for targeted mutagenesis by homologous recombination [Schaefer, 2002; Schaefer and Zryd, 1997]. The complete sequence of its genome has recently been established [Rensing et al., 2008] and it is also amenable to the generation of knock-down mutants by RNA interference [Bezanilla et al., 2003, 2005]. The relative simplicity of its development provides an optimal situation to study differentiation events at the single cell level throughout its life cycle [Cove et al., 2006]. Spore germination or protoplast regeneration initiates a juvenile filamentous stage, the protonema that is formed by two distinct tip growing cell types; chloronema and caulonema. Chloronemata are the photosynthetic cells of the protonema: they contain more than 100 large chloroplasts, have cell walls perpendicular to the axis of the filaments and do not grow nor divide in the absence of light. Caulonemata are the adventitious cells involved in nutrient absorption and rapid colonization of the growing substrate, they contain few small chloroplasts, have oblique cell walls, and grow and divide in darkness. The developmental pattern of the protonema is further determined by the division rates of subapical cells that determine the branching level. This process is related to actin dynamics in moss protonema since it requires the effective migration of a centrally located nucleus to the apical part of a subapical cell where it determines the plane of division and initiates the formation of a new side branch cell. Transition to caulinary growth takes place in about 5% of caulonema side branch initials that differentiate into a primitive meristem, the bud. This bud will further differentiate in a leafy shoot or gametophore that carry single layer leaves displaying phyllotaxis along the axis of the shoot. Filamentous basal and aerial rhizoids further differentiate from shoot epidermal cells: like caulonemata, rhizoids grow and divide in darkness and are involved in nutrient absorption and substrate fixation.

Five mutants of *P. patens* that show alterations of actin organization have been recently characterized. Abolition of tip growth in protonemal cells was the most visible common phenotype observed after deletion of ARPC4 [Perroud and Quatrano, 2006], of BRICK1 (a member of the Scar/Wave complex [Perroud and Quatrano, 2008]) or after knock-down (KD) of ARPC1

[Harries et al., 2005], of profilin, PRF-KD [Vidali et al., 2007] or of actin depolymerization factor, ADF-KD [Augustine et al., 2008]. Yet, differences were also observed between these mutants: PRF-KD and ADF-KD are dramatically affected in both cell growth and division processes and rapidly dies, whereas the other mutants are viable, and almost normal gametophores differentiate in ARPC4-KO and BRICK1-KO but not in ARPC1-KD. Successful differentiation of caulonema and rhizoid in ARPC4-KO, BRICK1-KO and ARPC1-KD also leads to controversial data. In vivo localization of Brick1 and Arpc4 at the tip of growing cells has been demonstrated, but a complete characterization of the actin network in such mutants has not yet been performed.

We report here the characterization of a knock-out mutant of the ARP3A gene of *P. patens* and provide a detailed description of the impact of this mutation on the structure of the actin cytoskeleton during moss development. Loss-of-function of Arp3 dramatically affects protonema development, abolishing tip growth in chloronema cells and blocking further differentiation of caulonemata. Yet, buds form normally and develop into slightly stunted gametophores that failed to differentiate rhizoids. In vivo analysis of the actin cytoskeleton in ARP3-KO reveals that this phenotype correlates with the absence of the localized F-actin arrays that are seen in WT at the tip and the bulging sites of filamentous cells, and in juvenile cells of regenerating leafy shoots [Finka et al., 2007]. We conclude that the ARP3-KO phenotype share many similarities with that of ARPC1-KD and ARPC4-KO which probably reflects loss of function of the whole Arp2/3 complex, and that the complex is necessary for the formation of localized F-actin arrays that are essential to establish tip growth in filamentous cells and contributes to elongation processes in the leafy shoot.

MATERIALS AND METHODS

Plant Tissue Culture, Transformation of Protoplasts and Selection of Resistant Clones

P. patens was grown axenically on solid minimal medium [Ashton and Cove, 1977] supplemented with 2.7 mM ammonium-tartrate (Merck Biosciences, Nottingham, England, UK)) and 25 mM glucose (Sigma, St. Louis, MI, USA) and under defined light conditions of 16 h of light and 8 h of darkness at 25° ± 1°C. Gametophores growth was conducted on solid minimal medium without supplement. Isolation of protoplasts and polyethylene glycol-mediated transformation were performed according to [Schaefer and Zryd, 1997]. For the dark grown experiments, fragments of 10-day-old moss tissue composed of protonemata and juvenile gametophores were grown in darkness on solid minimal medium supplemented with ammonium-tartrate and glucose in vertically positioned Petri dishes. For the phototropic and polarotropic experiments, freshly isolated protoplasts were embedded in top agarose and regenerated on solid protoplast medium. Low intensity white light ($5\ \mu E/m^{-2} \cdot s$) was provided unidirectionally for the phototropic response. For the polarotropic assays, embedded protoplasts were regenerated in glass Petri dish covered with a polarization filter; light intensity under the polarizing filter was adjusted to $5\ \mu E / m^{-2} \cdot s$.

Isolation and Detection of DNA

Genomic DNA was isolated using the cetyltrimethylammonium bromide method [Schaefer and Zryd, 1997]. The digested genomic DNA (3 μg per lane) was separated on a 0.7% agarose gel and blotted on Zeta-Probe membranes (BioRad, Hercules, CA, USA). Labeling of the probes (Amersham, Piscataway, NJ, USA) and membrane DNA blotting were performed according the manufacturer's protocols. High-stringency genomic DNA hybridization was performed at 65°C in 0.25 M sodium phosphate buffer pH 7.2 containing 7% SDS overnight and the membranes were washed 2 × 20 min with 0.1× SSC , 0.1% (w/v) SDS. Finally, the membranes were exposed to X-Omat AR film (Kodak, Hertfordshire, UK).

Cloning of *Physcomitrella* ARP3a Genomic Sequence

All plasmid manipulations and bacterial transformations were performed by standard techniques [Sambrook et al., 1989]. *Arabidopsis* genomic DNA (gDNA) was used as a template to generate AtARP3 fragment by PCR with primers AtARP3-FW160 (5′-TGGCAAACTCAGCACAAC-3′) and AtARP3-R1073 (5′-GCAAGAACACGAGCATCAA C-3′). The amplified 2173 bp fragment was ^{32}P-labeled and employed as a probe to screen a *Physcomitrella* λZAP cDNA library [Girod et al., 1999] at low stringency. A partial cDNA was obtained and used as a probe to screen a *Physcomitrella* λFIXII genomic library [Stavros Bashiardes; The *Physcomitrella* EST Program (PEP), University of Leeds (UK) and Washington University in St Louis (USA)]. Positive lambda clones were identified and partially mapped by restriction analysis and Southern hybridization (not shown). Two XbaI fragment of 6.7 and 2 kb were subsequently cloned in vector pBS-SK (-) (Stratagene) and sequenced, confirming that the entire genomic Arp3a locus was carried by these two fragments.

Construction of ARP3a Gene Disruption Vectors

The 2874bp EcoRI/SacI portion of the 6.7 kb XbaI Pp-ARP3A fragment (GenBank Accession No. AM287016) was inserted in EcoRI/SacI digested

pGEM-T Easy vector (Promega) to generate pGEM3.0/EcoRI-SacI. A XhoI/NotI (blunted) fragment from pBSMDIIIb (Murielle Uze, unpublished) containing a 35S::hygromycin^R::CaMVter cassette was inserted into AvaI/EcoRV digested pGEM3.0/EcoRI-SacI to yield pGAKO-Hyg with preserved XhoI site. To construct pGAKO-neo, XhoI/SpeI fragment of pBSMDII that carries a 35S::kanamycin^R::CaMVter transcription unit was inserted into the XhoI/SpeI digested pGAKO-Hyg backbone.

Construction of Integrative Vectors for Overexpression in *Physcomitrella*

A 2kb fragment of the 108 genomic loci (REF Schaefer, 1997] was excised by XhoI/XbaI from pBS-108 vector and cloned in the corresponding sites of pBNRF (Schaefer unpublished) that carries a 35S::neo^R::CaMVter resistance cassette, resulting in pBNRF108. The maize ubiquitin 1 promoter, first exon and first intron [Christensen et al., 1992] was excised as HindIII/BamHI fragment of pUbiGUS (Uze, not published) and inserted in HindIII/BamHI pBS-SK (-) to generate pBSUbi. The expression vector pBSUbiNOS was constructed by insertion of SpeI/NotI *nos* polyadenylation sequence from pG35SDT (Finka, not published) into SpeI/NotI cut of pBSUbi. The cDNAs encoding Arp3 from *Physcomitrella* (gift of M. Hasebe; Genbank Acc. No. BJ183257) was used as a template to generate PCR fragment with forward primer 5′-CACCTGTTCCTGAGAT CTG**ATGCTACTCAACGTCCT**-3′ and reverse primer 5′-GGATC**CTAACATACCCTTG AAGACCGG**-3′. Similarly, *Arabidopsis* ARP3 cDNA (RIKEN pda08187, Genbank Acc. No. AY093149) was amplified with primers 5′-AATGATCA**ATGGATCCGACTTCTCGA**-3′ and 5′-TTACTAGT**TCAATACATTCCC-TTGAA**-3′. PCR fragments were cloned in pGEM-T-easy (Promega) and sequenced. The Arp3 cDNA sequences were recovered by SpeI and cloned in SpeI cut pBSUbiNOS, resulting in overexpression vectors pBSUbiAtARP3 and pBSUbiPpARP3, respectively. Finally, the XmaI/SacII fragment of pBNRF108 carrying the selectable marker and the 108 targeting sequence was cloned at the corresponding sites Arp3 overexpression vectors, giving rise to the integrative vectors.

RT-PCR and PCR

Total RNA were isolated from a 3-week-old culture of *P. patens* using and the RNeasy plant mini kit (Qiagen, Hilden, Germany). The first strand synthesis was performed with M-MLV reverse transcriptase followed by PCR reactions using GoTaq® Flexi DNA polymerase (Promega). Confirmation of transcripts for the EST BJ183257 coding for PpArp3 was performed using the following primers: PpFab (5′-GAATACATGGGAGAAATCATGTTCGAG-3′), PpRA (5′-ATTTGTGGTCACCTCCAGATTTCTTT-3′), PpF-33 (5′-CTGCTGGATCCCTGATTCCCCTGTCG-3′), PpF-4 (5′-CGAGATGGATGCTACTCAACGTCCTGCTG-3′) and PpRC (5′-GAGGTC-GTGTAGCCAGCTGCTAGAAC-3′). The size of the amplified fragments that were obtained using the indicated combinations of the primers (Figs. 2D and 5C) perfectly matched those of the EST. In an attempt to detect predicted PpArp3b transcript primers PpFab and PpRB (5′- CTCTCTGACCACTCCCACTTTTGCTC-3′) were used. A partial genomic sequence of PpArp3a was determined by PCR using the same primers PpFab and PpRA, whereas genomic fragment of PpArp3b was amplified using PpFab and PpRB. As a control for RT-PCR moss tubulin fragment was detected using the primers TubF (5′-TGTGCTGTTGGACAATGAG-3′) and TubR (5′-ACATCAGATCGAACTTGTG-3′). The overexpression of *Arabidopsis* Arp3 transcript was confirmed using the primers AtF1 (5′- ATGGATCCGACTTCTCGACCCG-3′) and AtR1 (5′- TCACGACATTAACCTCCACCGG-3′).

Live Cell Microscopy and Image Analysis

The moss tissue was photographed using a Leica Diaplan microscope (Leica) coupled with DC300 digital camera (Leica) and acquired by IM50 software (Leica). The measurement of cell and tissue length as well as leas area was made by ImageJ software (http://rsb.info.nih.gov/ij/). The GFP-Tn was induced in moss tissue as it has already been described [Finka et al., 2007]. For confocal microscopy, carefully excised pieces of cellophane containing undamaged moss tissue were transferred into the glass slide chamber (Lab Tek II, Nunc) in inverted position and covered by block of solid medium. Confocal microscopy was performed on a TCS SP2 system using inverted microscope (Leica-DMRE). A krypton-argon laser (488-nm line) was used to distinguish between the GFP fluorescence and red autofluorescence of chloroplasts. The bandwidth mirror settings for discriminating between the two signals were 504/531 for GFP and 634/696 for chloroplasts. The two channels were allocated false green (GFP) and red (chloroplast) colours. Only the projections of image stacks showing GFP signal were processed using Photoshop 6.0 software and presented (Adobe Systems, Mountain View, CA).

RESULTS

Characterization of *P. patens* Arp3 Genes

The original genomic Arp3 fragment used in this study was isolated by heterologous screening from a lambda genomic library (Fig. 1A, see Material and

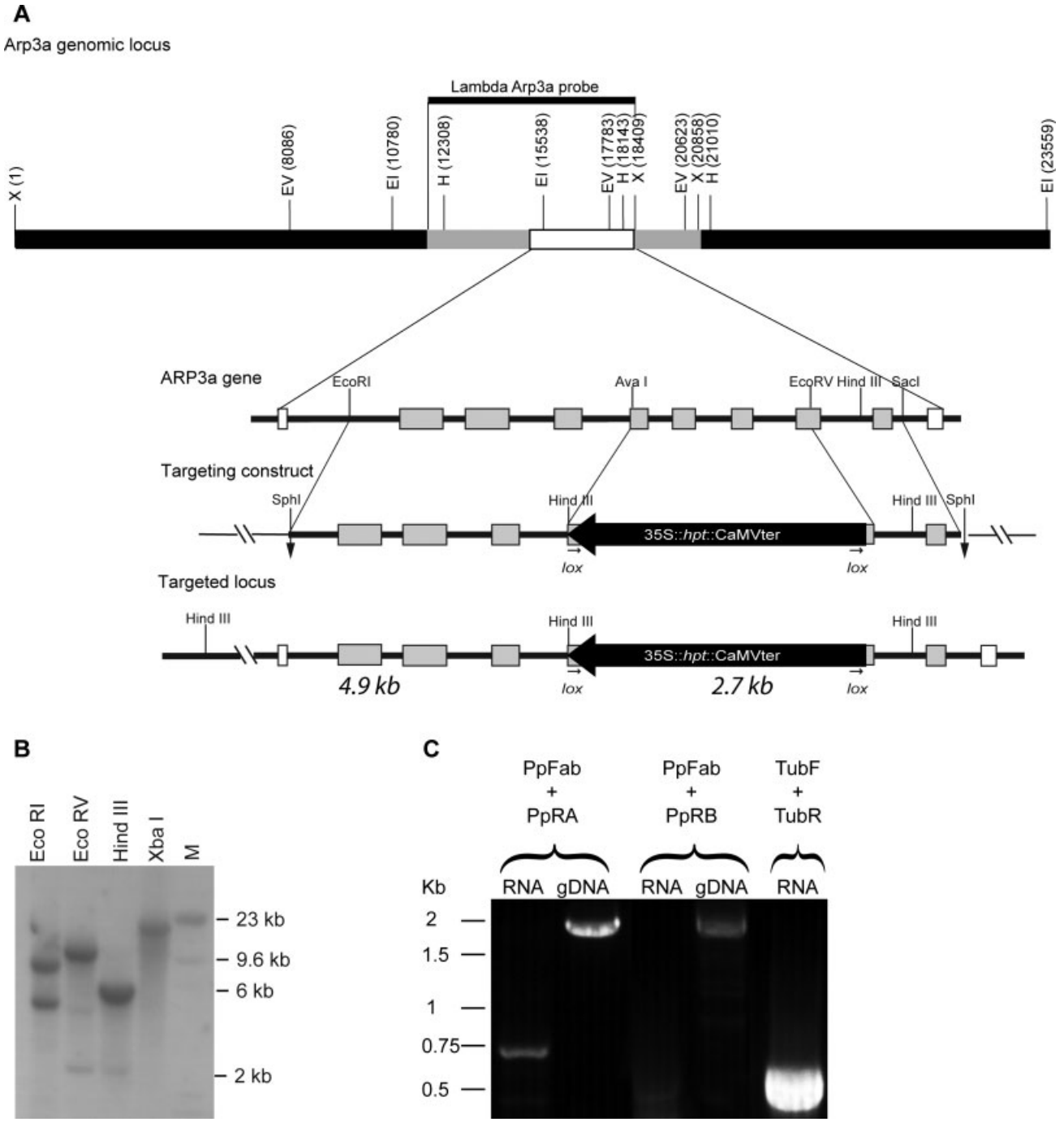

Fig. 1. Molecular analysis of *P. patens* ARP3a gene. (**A**) Schematic representation of the genomic locus of PpARP3a, of the derived vectors used in this study and of the disrupted PpARP3a locus by homologous recombination. The white box corresponds to the PpARP3a genomic sequence from start to stop codon, the grey bar to the fragment obtained from lambda Arp3a genomic clone and the black bar is reconstructed from the data of the whole genome (scaffold 85, 1163599 - 1187162). Restriction sites for the enzymes used in Southern analysis are marked (*Eco RI:* EI, *Eco RV:* EV, *HindIII:* H and *XbaI:* X). The black bar represents ARP3a genomic portion in lambda DNA that was used as a probe in B. In the knock-out vectors, the genomic ARP3a *AvaI* / *EcoRV* 906 bp fragment carrying exons 5–8 (grey boxes) was deleted and replaced by a hygromycin (black arrow) or a neomycin resistance cassette (not shown). Sequence homology with the target locus covers 1438 bp and 524 bp. Vectors were linearized at *Sph I* restriction sites prior to transformation. (**B**) High-stringency Southern blot analysis of wild type *P. patens* genomic DNA hybridized with the lambda PP-Arp3a genomic probe. The observed profile (RI 8035 and 4759 bp, RV 9797 and 2740, H 5833 and 2869 and X 18410) confirmed that the Arp3a sequence is unique. Marker (M) was lambda DNA digested with Hind III. (**C**) RT-PCR and PCR from WT total RNA and gDNA, respectively Primers PpFab and PpRA were used to amplify putative *arp3a* (lane 1 and 2), while PpFab and PpRB were used to detect predicted *arp3b* sequence (lane 3 and 4). Amplification of a tubulin fragment was used as a template control for RT-PCR (lane 5).

Methods for details). Its sequence was established and Southern blot analysis confirmed its presence as a unique sequence in the moss genome (Fig. 1B). A search of the moss EST databases (PhyscoBase and NCBI ESTs) reveals the presence of seven homologous sequences from both protonemal and gametophytic tissue (not shown). A full-length cDNA clone (pphb36p18, accession BJ588569 and BJ183257) was obtained from the NIBB Okasaki moss EST collection and sequenced. We could establish that the genomic structure of the Arp3 gene is organized in 10 exons, and exons V to VIII were replaced by the selectable cassette to generate the knockout vectors (Fig. 1A). We search the recently published whole genome of *P. patens* for the presence of Arp3 related sequences and identified two putative ARP3 loci located on distinct genomic scaffolds (http://genome.jgi-psf.org/Phypa1_1/Phypa1_1.home.html). Scaffold 85 (coordinates 1177835-1181287) corresponds to the Arp3

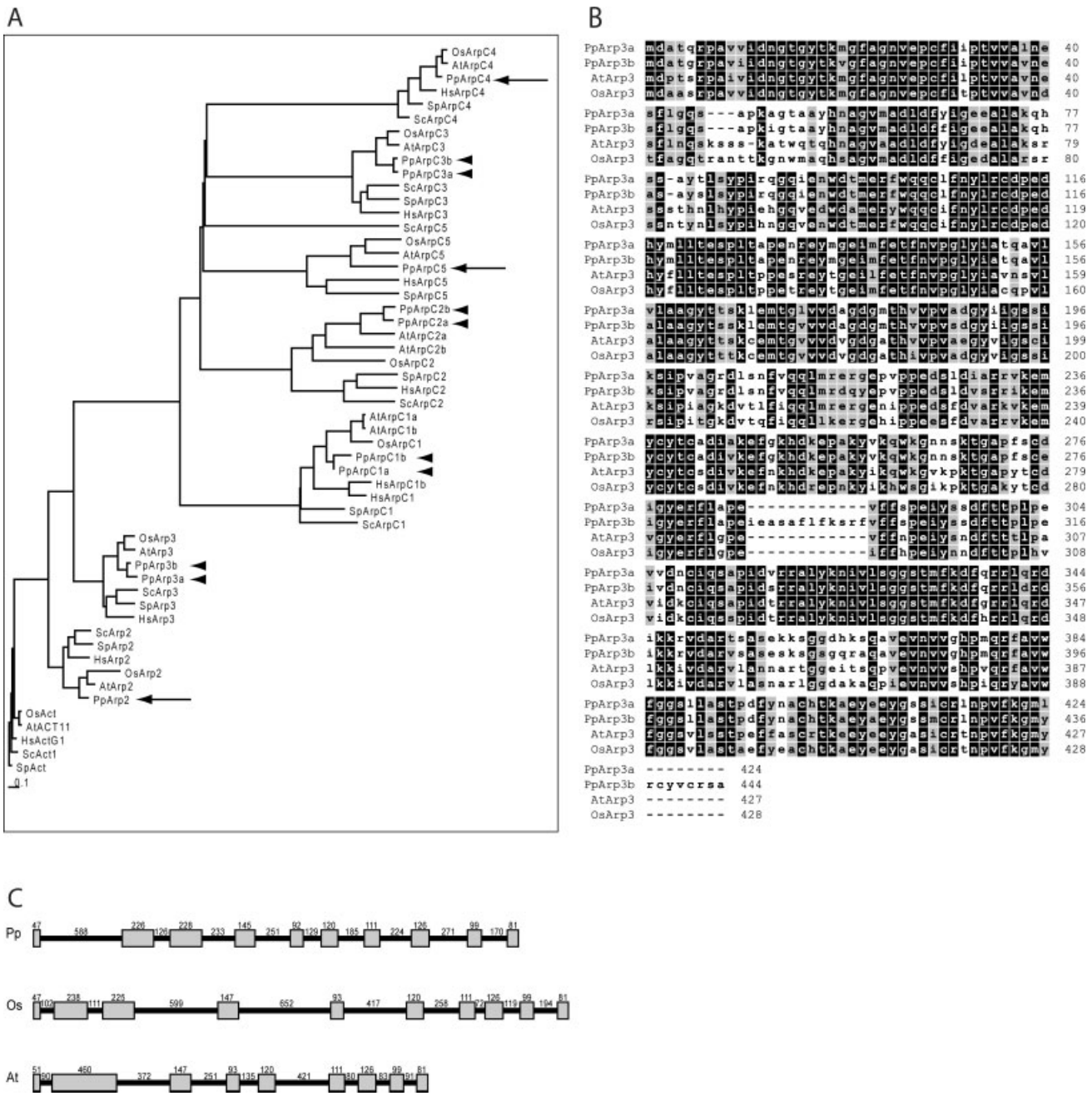

Figure 2.

sequence described above and will be further referred to as Pp-ARP3A, and scaffold 110 (coordinates 1228340-1231825), which we further call ARP3B. The predicted coding sequence of Arp3b shares 60% nucleotide identity with Arp3a and encodes a putative protein of 444 amino acid residues, sharing 88.3% identity with the predicted Arp3a amino acid sequence (Fig. 1C). Yet, we could not find Arp3b homologous EST in the moss EST databases nor amplify a putative Arp3b cDNA by RT-PCR (Fig. 1D). We conclude that the ARP3B locus probably carries a putative pseudo gene generated by a recent genome duplication that is not transcribed in moss wild type.

Comparison of the genomic and cDNA sequence established that the moss ARP3A gene (GenBank Accession No. AM287016) was encoded by10 exons (Fig. 2A). The same number of exons is present in the rice ARP3 gene ortholog (Genbank Acc. No. AP004092), whereas the *A. thaliana* ARP3 gene (Genbank Acc. No. At1g13180) has nine exons. The *A. thaliana* second exon corresponds to the combined second and third exon of rice and *P. patens*. The individual size of the last five exons is equal in all of these orthologs, but the sizes of the introns are different (Fig. 2A). The derived amino acid sequence of Pp-Arp3a encodes a protein of 424 amino acids that share 76.3% and 75.2% identity with the *Arabidopsis* and rice Arp3 protein sequences, respectively (Fig. 2B). The genomic structure and the protein sequence of the moss ARP3A gene are thus highly similar to that of the *A. thaliana* and rice homologues.

Regarding genes encoding the seven subunits of the Arp2/3 complex, examination of the complete genome sequence of *P. patens* identified orthologs for the seven subunits. The Arp2, ArpC4 and ArpC5 proteins are encoded by single genes, whereas the genes encoding the other subunits are duplicated. These genes are actively transcribed since ESTs corresponding to all but two of them (Arp3b and ArpC2 (e_gw1.249.24.1 [Phypa1_1: 146870]) were found in the EST database. The relationship between *P. patens* Arp2/3 amino-acid sequences to each other and to known Arp2/3 sequences from animals and fungi was explored using protein sequence comparison algorithms, such as the neighbor-joining tree shown (Fig. 2C). All sequences are clear orthologs of the Arp2/3 complex proteins from many organisms, sharing high percentage of amino acid sequence identity with plant orthologs. Taken together, these data show that sequences of the Arp2/3 complex are highly conserved from moss to humans, suggesting that the function of the Arp2/3 complex may also be highly conserved.

Disruption of PpARP3a Alters Cellular Elongation and Blocks the Differentiation of Caulonemata and Rhizoids

To investigate the role of Arp3a in moss development, loss-of-function mutants were generated by targeted mutagenesis in the wild type (WT) strain. The mutated *arp3a* lines were generated using linearized pGAKO-hygro (Fig. 1A). During the antibiotic selection

Fig. 2. Structural and phylogenetic relation of the *Physcomitrella* Arp3 genes with plant Arp3 sequences and with other subunits of Arp2/3 complex. (**A**) Phylogenetic relationships of Arp2/3 complex subunits and actin proteins. Plant, fungal and animal protein sequences of the seven subunits of the Arp2/3 complex are compared in a neighbor-joining (NBJ) tree. The tree is rooted to highly conserved conventional actins. The tree shows that each subunit of Arp2/3 complex assemble into a distinct clade that brings together yeast, animal and plant sequences, and that moss sequences occupy a ancestral position within a distinct subclade of plant sequences. The moss *P. patens* contains two sequences encoding Arp3, Arpc1, Arpc2 and Arpc3 subunits (arrowheads), but only one sequence for Arp2, Arpc4 and Arpc5 (arrows). In the tree, the accession numbers of moss protein sequences were given using *Physcomitrella* genome server (http://genome.jgi-psf.org/cgi-bin/searchGM?db= Phypa1_1) and for the rest of protein encoding sequences the NCBI accession numbers were used as follows. Moss: PpArp2, estExt_gwp_gw1.C_170236; PpArp3a, estExt_fgenesh1_pm.C_850013; PpArp3b, e_gw1.110.59.1; PpArpC1a, estExt_fgenesh1_pg.C_200201; PpArpC1b, estExt_Genewise1.C_170033; PpArpC2a, e_gw1.34.164.1; PpArpC2a, e_gw1.249.24.1 PpArpC3a, estExt_fgenesh1_pg.C_141001; PpArpC3b, estExt_gwp_gw1.C_470079; PpArpC4, estExt_fgenesh1_pg.C_2040035; PpArpC5, estExt_fgenesh1_pm.C_830007. Human: HsActG1, NP_001605.1; HsArp2A, NP_001005386; HsArp3, NP_065178.1; HsArpC1a, NP_006400.2; HsArpC1b, NP_005711.1; HsArpC2, NP_005722.1; HsArpC3, NP_005710.1; HsArpC4, NP_005709.1, HsArpC5, NP_005708.1. Brewer yeast: SpAct1, NP_595618.1; SpArp2, NP_001018288.1; SpArp3, NP_065178.1; SpArpC1, NP_595909.1; SpArpC2, NP_593903.1; SPArpC3, NP_596291.1; SpArpC4, NP_594116.1; SpArpC5, NP_593727.1. Baker yeast: ScAct1, NP_116614.1; ScARP2, NP_010255.1; ScARP3, NP_012599.1; ScArpC1, NP_009793.1; ScArpC3, NP_013474.1; ScArpC4, NP_012912.1; ScArp5, NP_012202.1. *Arabidopsis*: AtACT11, NP_187818.1; AtArp2, NP_189336.1; AtArp3, NP_172777.1; ArpC1a, NP_180648.1; ArpC1, NP_180688.1; AtArpC2a, NM_102820.2; AtArpC2b NM_179877.1; AtArpc3, NP_564757.1; AtArpC4, NP_001031632.1; AtArpc5, NP_567216.1. Rice: OsAct, NP_001054419.1, OsArp2, NP_001061655.1; OsArp3, NP_001047323.1; OsArpC1, NP_001048519.1, OsArpC2, NP_001053297.1; OsArpc3, NP_001046384.1; OsArpC4, lNP_001051892.1; OsArpc5, NP_001068095.1 (**B**) Alignment of *P. patens* (Pp), rice (Os) and *A. thaliana* (At) Arp3 amino acid sequences. Black and grey boxes highlight identical and similar residues, respectively. In the predicted PP-arp3b protein, the alignment reveals the presence of a stretch of 12 amino acids at position 286 that matches with the junction between exon VI and VII. An acquired mutation within a splicing site or a stop codon could be the origin of its pseudogene status. (**C**) Schematic representation of the organization of plant ARP3 genes in *P. patens* (Pp), rice (Os) and *A. thaliana* (At). The overall organization of the three genes is highly similar except that the moss and rice exon II and III are encoded by the exon II in *Arabidopsis*. The rectangles represent exons. Introns are presented as lines. The numbers represent lengths in base pairs.

process, more than a hundred indistinguishable phenotypic mutants could be visually identified by their very compact growth pattern. We confirmed, by Southern blot analysis, that this phenotype is associated with the effective disruption of the moss ARP3a gene (Fig. 3a).

A detailed phenotypic characterization over the entire life cycle of the moss *arp3a* mutants was performed. Whereas wild type juvenile protonemata spread evenly on the agar surface and were composed of elongated chloronemata and caulonemata (Figs. 3bB and 3bF), juvenile protonemata from the *arp3a* knock-out were extremely compact and apparently composed of a single type of almost cubic cells (Figs. 3bA and 3bE). These cells were filled with numerous chloroplasts and separated by cell walls perpendicular to the axis of the filament, two criteria that define chloronemata. To characterize this compact phenotype, a detailed morphometric analysis was performed on more than 30 individual WT and *arp3a* mutated cells regenerated from isolated protoplasts. This analysis showed that the width of the filament was similar in both strains, but that the width to length ratio was dramatically affected in mutant cells (1:2 in *arp3a*, 1:5 in WT, data not shown). We also observed a significant decrease of the branching level of the protonema in the *arp3a* mutant: the probability of subapical cells to undergo a second division to form side branches is almost one in WT, but hardly reaches 0.25 in *arp3a* (Figs. 3bA, 3bB, 3bE and 3bF and data not shown), indicating that the rate of cell division of subapical cells is affected by the mutation. Yet, mitoses were correctly located at the tip of apical cells and at the apical part of subapical cells (Fig. 3bE). These data indicate that the *arp3* mutation specifically affects tip growth but not cell polarity in protonemal cells. To investigate the role of Arp3a in protoplast regeneration and tropic growth responses, protoplasts of WT and *arp3a* strains were regenerated under standard, unidirectional and polarized white light. Regeneration rates, phototropic and polarotropic responses were comparable in both strains, indicating that the ARP3A gene was dispensable for these processes (Figs. 3bI and 3bJ and data not shown).

Detailed observation of the cellular composition of the protonema suggested that it was exclusively composed of chloronemata that were unable to differentiate into caulonemata. Since caulonemata are the only cell type of WT moss protonema that can grow and divide in darkness, we grew both strains in darkness to verify whether caulonemata were present or absent in *arp3a* mutant. We could not detect any caulonemata in mutant lines, whereas they developed in WT tissue, but etiolated gametophores developed normally in both strains, indicating that *arp3a* is neither required for dark growth nor for gravitropic responses (Figs. 3bK and 3bL). It has been demonstrated that development of caulonemata can be induced by auxin, such as 1-naphtalen acetic acid (1-NAA) in light grown chloronema tissue [Imaizumi et al., 2002]. When 1week old tissue of *arp3a* mutated strains was treated with 1-NAA in concentrations ranging 1–10 μM to try to induce caulonemata, no formation of caulonemata was observed (data not shown). Taken together, these data suggest that arp3a dependent establishment of tip growth is necessary for the differentiation of caulonemata from chloronemata.

Consequently, the absence of caulonema cells results in the direct differentiation of buds from chloronema side branch initials in the mutant, whereas they commonly developed from caulonema side branch initials in wild type (Figs. 3bG and 3bH). Bud formation occurred simultaneously and at equal frequencies in the mutants and in wild type, and their morphology was apparently not affected. These buds further differentiated into leafy shoots that were similar to wild type shoots except for two features: (a) *arp3a* gametophores were slightly stunted and carried smaller leaves than the WT (Fig. 3bM), and (b) aerial and basal rhizoids that normally differentiate from stem epidermal cells have never been observed in mutant gametophores (Figs. 3bN and 3bO). The absence of both caulonema and rhizoids completely impedes attachment of the mutant colony to the growth substrate, leading to the formation of spherical colonies of leafy shoots that roll in the Petri dish (Figs. 3bC and 3bD). Yet, phyllotaxis and the general architecture of the leafy shoot were not affected. The size alterations in the gametophores were measured on more than twenty wild-type and mutated *arp3a* lines grown for 6 weeks on solid minimal medium. In fully differentiated shoots, the mean lengths of the internodes were 0.20 ± 0.02 mm in wild type and 0.15 ± 0.02 mm in the mutant, whereas the areas of adult leaves were 0.85 ± 0.2 mm^2 and 0.53 ± 0.1 mm^2 in wild type and the mutant, respectively. Yet the number of cells per internode and per individual leaves was similar in both strains (data not shown). We conclude that the stunted aspect of the *arp3a* mutant gametophore is associated with reduced expansion of shoot and leaf cells. Fully differentiated WT and mutant colonies were grown for 15 weeks on minimal medium in short day (8 h light a day) and low light intensity (15 $\mu E / m^{-2} \cdot s$) to induce sporogenesis. Antheridia and archegonia differentiated normally on both strains, but we never observed any differentiated spore capsule in *arp3a* mutant (data not shown).

Thus our phenotypic analysis shows that disruption of moss ARP3A gene impairs cellular elongation of chloronema cells and completely stops their further differentiation into caulonemata in the protonema. Gametophores are less affected by the mutation but display a stunted phenotype associated with smaller

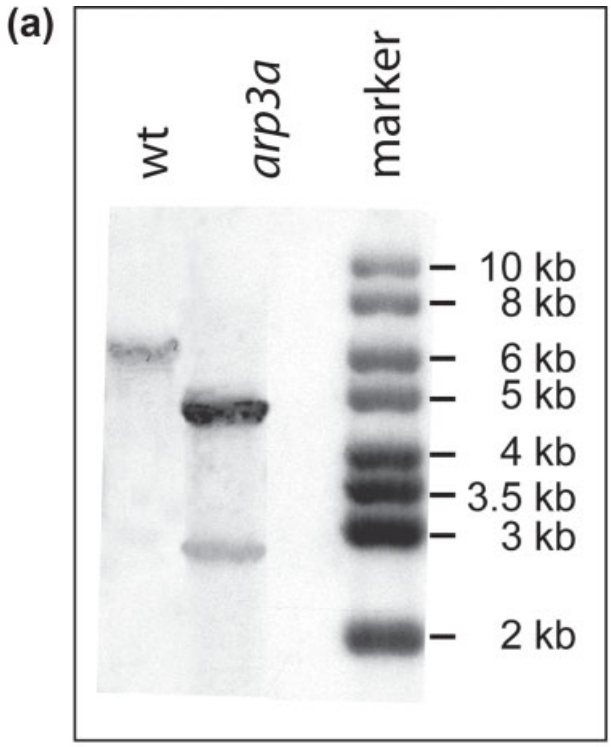

Fig. 3. (**a**) DNA gel blot analysis of genomic DNA from moss wild-type (wt) and *arp3a* strain. Three microgram of genomic DNA of *P. patens* was digested with *Hind III*. Entire ARP3a cDNA was used as a probe. Molecular mass markers are given at left in kilobase pairs. (b) Comparison of the phenotypic characters of wild type and *arp3a* strains of *P. patens* at different developmental stages. Two weeks and 4 weeks old colonies of *arp3a* mutant (**A**, **C**) and of wild type (**B**, **D**), respectively. (**E**) The *arp3a* mutant has filament made of short chloronemal cells. (**F**) Chloronemal filament of wild type consists of elongated cells. (**G**) In *arp3* strain, buds appear directly on the shortened chloronemal cells with no caulonemal phase. (**H**) In wild type, buds appear on caulonemal cell with oblique cell walls. Freshly isolated protoplasts of *arp3a* mutant (**I**) and wild type (**J**) are grown under polarized light for 10 days, chloronema align with the electrical vector (horizontal). In 10 days old dark grown moss tissue, caulonemal filaments are absent in the *arp3a* lines (**L**), but present in wild type (O). Negatively gravitropic etiolated buds from *arp3a* mutant (arrowheads) are similar to that of the wild type (L, inset); the gravity vector is presented by arrows. (**M**) Four weeks old leafy shoots of *arp3a* mutant and wild type. Detailed image shows there are no rhizoids at the base of the *arp3a* mutant leafy shoot (**N**), whereas there is developed rhizoid network at the base of the wild type gametophore (**O**) Negatively gravitropic etiolated buds from *arp3a* mutant (arrowheads) are similar to that of the wild type (O, inset); the gravity vector is presented by arrows. The isolated protoplasts of *arp3a* (N) mutant and wild type (**Q**) are grown under unidirectional light and show positive phototropism; light source from right (arrows). Bars (A, B, N, O) 500 μm; (C, D, K, L), 10 mm; (E-H) 100 μm; (I, J) 200 μm; (M) 1 mm.

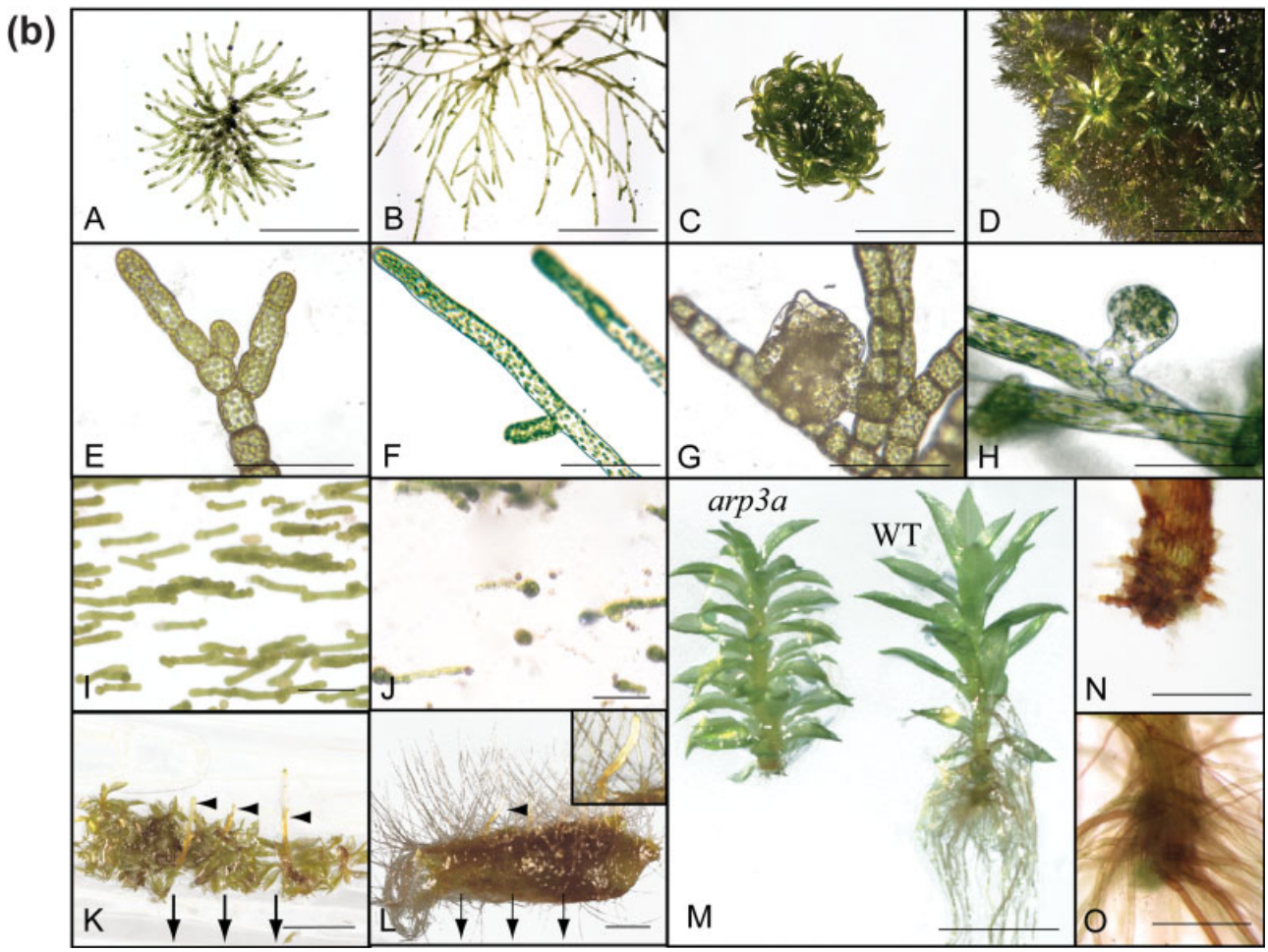

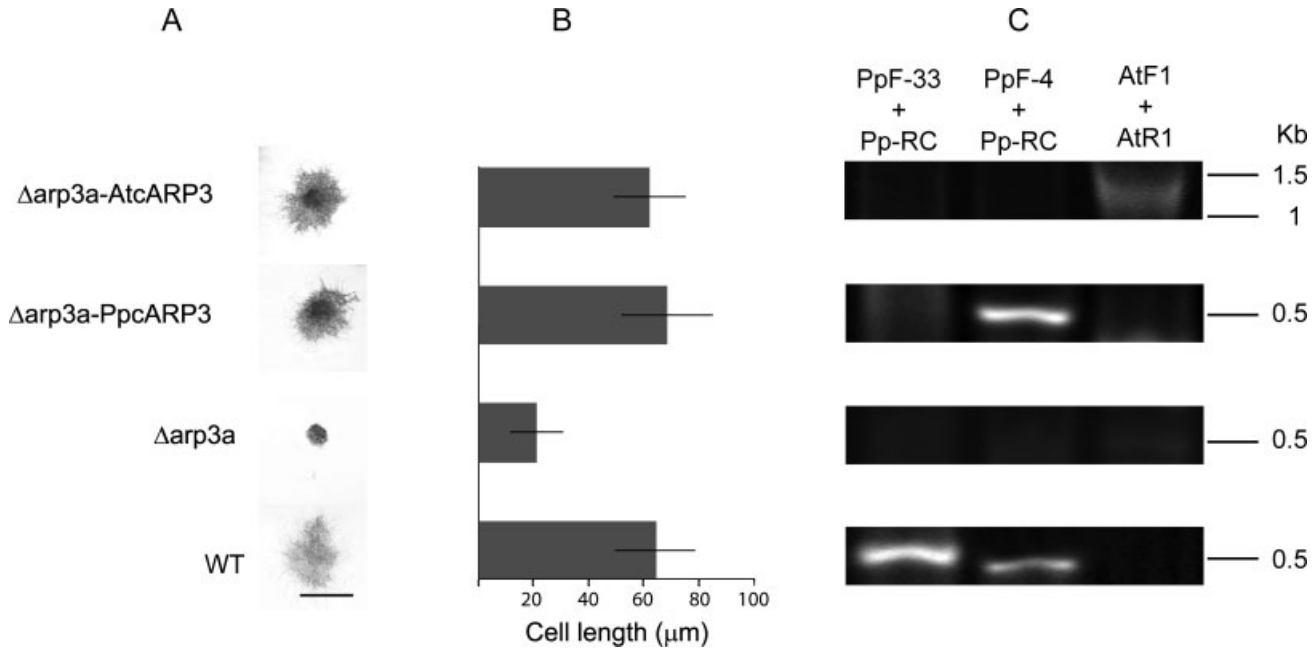

Fig. 4. The *arp3a* mutant phenotype is fully complemented by the expression of Arp3 cDNA from both *P. patens* and *A. thaliana*. (**A**) The panel represents a low magnification view of three-week-old colony from WT, Δarp3a and of Δarp3a strains complemented with either moss or *Arabidopsis* Arp3. Bar: 1 cm. (**B**) The *arp3a* mutant phenotype results from a reduction in cell elongation. We determined the mean cell length of apical cells measured in one-week old colonies of the same strains depicted in (A). Mean ± SD ($n \geq 30$ cells for each strain). (**C**) RT-PCR from total RNA extracted from three-week old tissue from the same strains. To distinguish Arp3 WT transcript from the mRNA generated by PpcARP3, we used primer PpF-33 which anneals with the WT but not with the PpcARP3 transcript. Expression of the cDNAs correlates with phenotypic complementation.

cells whereas formation of filamentous rhizoids is blocked. Noticeably, the mutation also induces a sterility phenotype. The main consequence of the absence of caulonemata and rhizoids is the inability of the plant to colonize the growing surface efficiently and to adhere to the substrate.

Complementation of the *arp3a* Mutation by the Moss and *Arabidopsis orthologs*

Complementation of the *arp3a* mutation with the Arp3 cDNA from *P. patens* and *A. thaliana* was attempted to demonstrate the specificity of the phenotype and to address the level of functional conservation of the protein between different species. We constructed vectors containing the cDNA of Arp3 from *P. patens* or *A. thaliana* driven by the maize ubiquitine-1 gene promoter, a neomycin resistance cassette and a fragment of the 108 genomic loci as targeting sequence. An *arp3a* mutant strain was retransformed with these vectors and G-418 resistant plants were selected. During the initial selection, we could visually identify complemented colonies by their unrestricted growth pattern following transformation with the moss and the *A. thaliana* expression vectors. Three complemented colonies of each transformation were further selected for phenotypic characterization. In the complemented strains, the overall morphology of the colony is normal (Fig. 4A) and the mean length of apical cells is comparable to the WT (Fig. 4B). The protonema is composed of normally elongated chloronemata and caulonemata, and buds differentiate from caulonema side initials. Filamentous growth and gravitropic responses of caulonemata in dark grown cultures were similar to the wild type strain and gametophores did not display anymore the stunted phenotype observed in the *arp3a* mutants (data not shown). At the molecular level, we could correlate restoration of the WT phenotype with specific expression of the complementing expression cassette (Fig. 4C). These data demonstrate that the mutant phenotype described above is effectively associated with *arp3* loss-of-function and can be complemented by both the *Arabidopsis* and *Physcomitrella* ARP3 genes.

Actin Organization in *arp3a* Mutant Lines is Affected

The consequence of loss of function of the ARP3a gene on the organization of the actin cytoskeleton was studied in the previously described HGT1 strain that carries a heat shock inducible GFP-talin reporter construct [Finka et al., 2007; Saidi et al., 2005]. The Hyg^R HGT1

strain was transformed with by pGAKO-neo (see Materials and methods), G-418 resistant *arp3*a colonies were visually identified during selection and four of them were isolated for further analysis. The phenotype of these colonies could not be distinguished from that of *arp3a* strains obtained in a WT background (not shown). Preliminary experiments confirmed that a 1 h heat-shock at 37°C was sufficient to obtain an efficient and comparable in vivo labeling of the F-actin network in both HGT1 and *arp3a*-HGT1 strains without affecting their morphology. It was recently reported that F-actin structures could be reversibly destroyed in *Arabidopsis* root epidermal cells by a heat shock stress [Muller et al., 2007]. To investigate whether the same process takes place in moss, tissue from the HGT1 strain that had been induced 16 h before was resubmitted to a heat shock and observed within the next 2 h by confocal microscopy. In actively growing cells, F-actin apical and perinuclear arrays and fine cortical cables were comparable to those observed in the untreated samples. Yet we observed a partial degradation a cortical thick actin bundles in differentiated leaf cells that was fully reversible within the next 5 h (data not shown). We concluded that the HS treatment was not detrimental for the F-actin cytoskeleton under the experimental conditions used in this study.

In the protonema, the most striking difference observed between HGT1 and the *arp3a* HGT1 cells was the complete absence in the mutant of F-actin star-like cap arrays connected with the cortical cables that form at the growing tip and at the site of new side branch initials in WT (Figs. 5A, 5B, 5E and 5F) [Finka et al., 2007]. Yet, the complex network of fine cortical cables that often displayed an apicobasal gradient of bundling (Figs. 5C and 5D), the perinuclear meshwork and the cellular compartmentation with F-actin containing cytoplasmic strands were comparable in juvenile cells of both strains (data not shown). A subtle difference was detected in older subapical cells: cortical cables in HGT1 often form large bundles that were not observed in *arp3a* mutated cells (not shown).

In juvenile buds, the numerous F-actin cortical star-like arrays that are observed in HGT1 were totally absent in *arp3a* strains whereas the other F-actin structures were unaffected (Figs. 6A and 6B). In juvenile leafy shoots, binocular observation in epifluorescence showed that in both strains, the basis of the stems and the leaves was more densely labeled with GFP than the upper part carrying fully differentiated leaves (data not shown). The presence of a more complex network of F-actin structures within this area, where active growth processes take place, was confirmed by confocal observation. In HGT1, a dense network of cortical cables predominantly oriented perpendicularly to the axis of the cell was observed in both basal stem and leaf cells (Figs. 6D and 6G). This network was intimately associated with one or few star-like cap arrays frequently located at the apical pole of the cell and displaying the same predominant orientation. The same cortical network was observed in *arp3a* strains but star-like arrays were absent (Figs. 6C and 6E). In the leaf tip, that is composed of fully differentiated cells, the cortical network formed by large F-actin bundles in HGT1 was composed of much thinner cables in *arp3a* (Figs. 6F and 6H), as previously observed in older protonemal cells. Beside these differences, F-actin labeling around the nucleus and within cytoplasmic strands were similar in both strains.

Taken together, these data strongly suggests that the moss Arp3a gene is necessary to establish localized F-actin star-like cortical arrays that are directly connected with the network of cortical cables. These F-actin star-like arrays, which are reminiscent of the F-actin cap structure previously described in fission yeast, would be required to establish tip growth and control lateral branching in chloronemal cells, as well as localized cellular growth during meristematic development. The possibility that this function is performed by the entire Arp2/3 complex is very likely and will be discussed in the next section.

DISCUSSION

We describe here the loss of function phenotype of Arp3a in *P. patens*, a subunit of the Arp2/3 complex, and provide a detailed description of the impact of the mutation on the structure of the F-actin cytoskeleton throughout moss development. Two loci encoding for a putative Arp3 protein were identified in the moss genome but several lines of evidence indicate that only one of them is actively transcribed; (a) Arp3a but not Arp3b was successfully amplified by RT-PCR (Fig. 1), (b) several ESTs for Arp3a, but not for Arp3b could be identified in the 200000 ESTs deposited in the databases, (c) the predicted sequence of the Arp3b protein contains a stretch of 12 amino acids within a highly conserved domain and a C-terminal extension that could interfere with its function (Fig. 2), (d) loss of function of Arp3a alone generated the same developmental phenotype in WT and HGT1 strains, and (e) the phenotype was fully complemented by expression of the moss or the *Arabidopsis* ARP3 cDNAs (Fig. 4). We conclude that the mutation described here results from *arp3* loss of function.

The moss genome encodes for all seven subunits of the Arp2/3 complex and four of them are duplicated (Arp3, ArpC1, ArpC2 and ArpC3). Phylogenetic analysis revealed that the moss genes are highly similar to the plant, yeast and animal orthologs, and occupy a basal/ancestral position within a subclade of plant sequences,

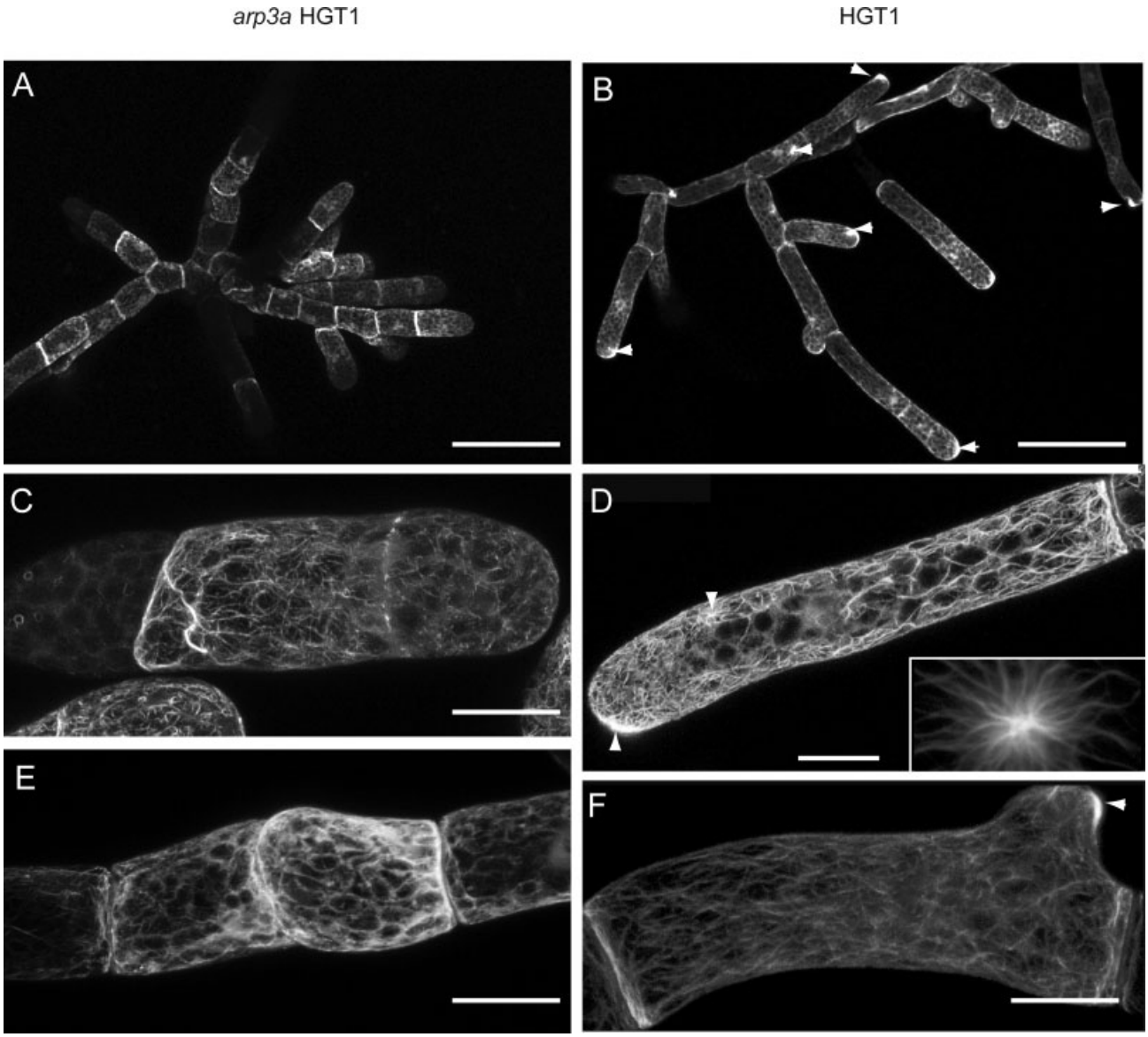

Fig. 5. Comparative CLSM images of protonema from *arp3a* HGT1 mutant (**A**, **C**, **E**) and HGT1 strain (**B**, **D**, **F**) overproducing GFP-talin. The cortical star-shaped F-actin arrays are only observed in HGT1 cells (arrow heads). Images are stacked Z projection of (A, B) protonemal filaments at ×20 magnification, (C, D) chloronemal apical cells at ×63 magnification, and (E, F) bulging sub-apical cells. The inset in (D) represents a magnified view of star-like actin array. Bars: (A, B) 100 μm; (C–F) 10 μm.

suggesting that these genes derive, at least in plants, from a common ancestor (Fig. 2). Protein sequence identity is over 70% with plant orthologs and above 50% with yeast and animal sequences, indicating a very high level of similarities which strongly supports a similar function for the complex. The presence of duplicated genes for some of the subunits is consistent with the evidence of a whole genome duplication that occurred about one and a half million years ago *in P. patens* [Rensing et al., 2008].

The most obvious phenotype of *arp3a* strains is the dramatic reduction of tip growth in filamentous cells, and to a lesser extent in growth of leafy shoots which are stunted (Fig. 3b). In addition, the branching level of filaments is reduced and differentiation of caulonemata and rhizoids from chloronemata and stem epidermal cells, respectively, is completely abolished. Yet, tropic responses are normal and mitoses properly located in the apical pole of filamentous cells. These data suggest that the *arp3* mutation could affect the organization of domains of localized cell expansion. In protonema, these domains are required for tip growth and differentiation of adventitious caulonemata, accounting for the strong

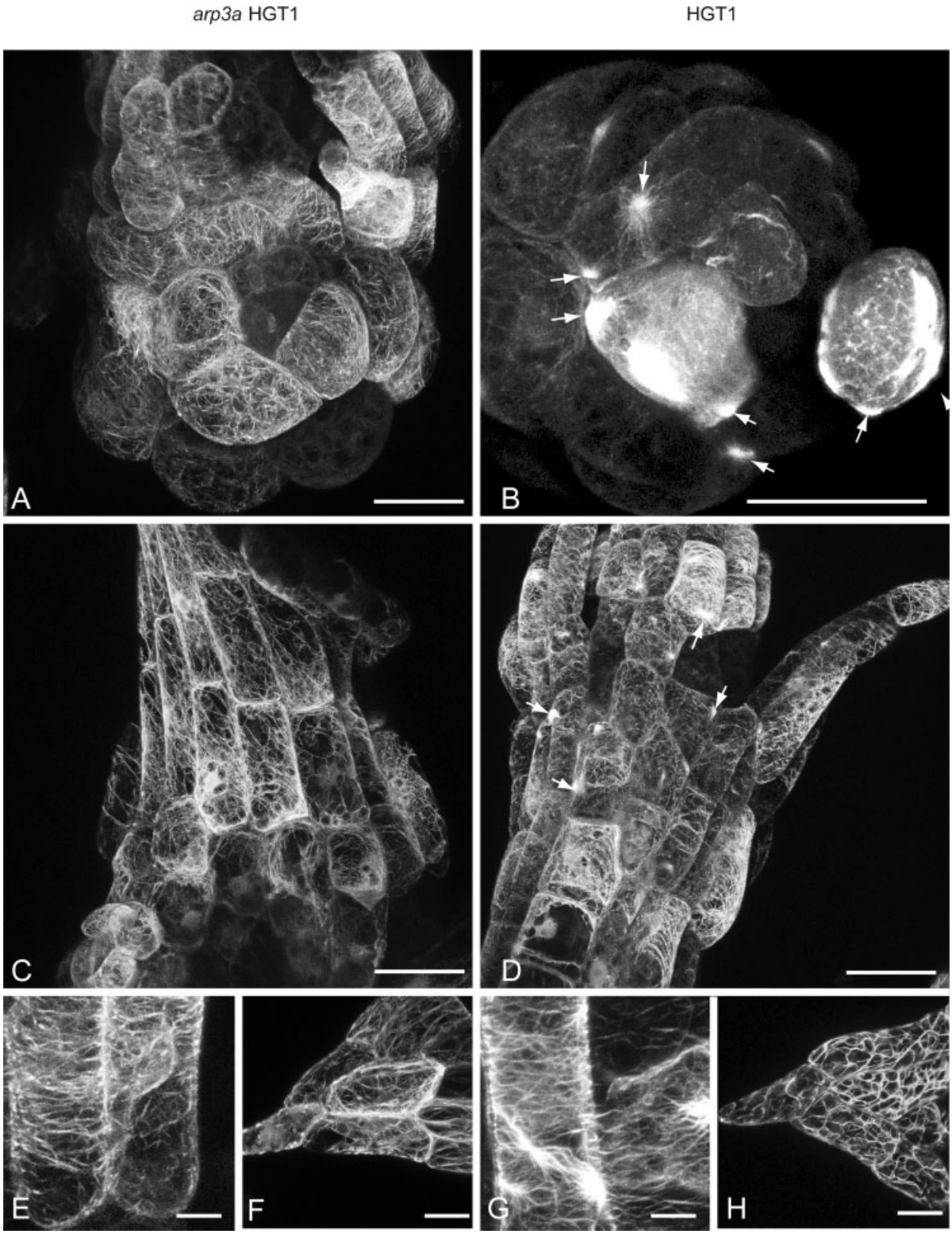

Fig. 6. Comparative CLSM images of buds and leafy shoots of *arp3a* HGT1 (**A**, **C**, **E**, **G**) and HGT1 strains (**B**, **D**, **F**, **H**) overproducing GFP-talin. Images are stacked Z projection of: (A, B) apical view of young meristem with juvenile leaf primordia (×63), (C, D) lateral view of young leafy shoots (×63), (E, F) basal cells of juvenile leaves (×63), and (G, H) tip cells of fully differentiated leaves (×63). The numerous F-actin cortical arrays (arrows) are only observed in HGT1. Predominant perpendicular orientation of fine F-actin cables can be seen in C, D, E and F whereas large F-actin bundles are only observed in HGT1 (H).Bars: (A–D, F, H) 20 μm; (E, G) 10 μm

protonema phenotype. But they play a minor role on the establishment of cell polarity since mitoses are properly oriented. In leafy shoots, these domains are necessary for rhizoids development and contribute in part to cell elongation, but are dispensable for the overall architecture of the shoot.

The *arp3a* phenotype is highly similar to that observed for mutants of two other subunits of the Arp2/3 complex, ArpC1-KD [Harries et al., 2005] and ArpC4-KO [Perroud and Quatrano, 2006]. Yet leafy shoots failed to differentiate in ArpC1-KD. This difference might reflect distinct functions of subunits within the moss Arp2/3 complex, as observed in fission yeast, or result from the RNAi approach used in that work, which had some additional phenotypic impact. Characterization of deletion mutants for ArpC1 and for the other subunits of the complex will unambiguously answer that question. Nevertheless, the phenotypic pattern described here and in these studies most likely represent the effect of loss of function of the whole Arp2/3 complex on moss development.

The *arp3a* mutation was brought into HGT1 strain [Finka et al., 2007] to determine changes in the structure of the F-actin cytoskeleton. We previously described F-actin structures during moss development and reported the presence of star like arrays of fine F-actin that are intimately connected with cortical cables at the growing tip of apical cells and at the bulging site of lateral branches. Similar structures were also observed in actively growing buds, leaf and stem epidermal cells. Detailed analysis of F-actin in *arp3* HGT1 strain revealed a major change in the F-actin cytoskeleton: cortical star shaped F-actin arrays were completely absent in actively growing cells of protonema and leafy shoots (Figs. 5 and 6). Yet, the overall organization of F-actin in a network of fine cortical cables and a perinuclear mesh of diffused F-actin connected with the cell cortex though cytoplasmic strands was essentially unaffected by the mutation. We thus identified a specific subfraction of F-actin structures that is lost in *arp3a* strains. Remarkably, using the same HGT1 reporter line to label F-actin, Perroud and colleagues have recently shown that these arrays were also specifically affected in protonemal cells of BRICK1-KO, but their presence in leafy shoots was not investigated [Perroud and Quatrano, 2008]. Such structures have already been observed at bulging sites in *Funaria* protonema stained with rhodamin phalloidin [Quader and Schnepf, 1989]. Yet, using Alexa-488 phalloidin staining, Augustine and colleagues observed star shaped apical arrays in ADF-KO but not in WT apical cells [Augustine et al., 2008]. Discrepancies between different F-actin labeling techniques in plant cells has been discussed recently [Yoneda et al., 2007], and in vivo labeling by inducible transient expression of the GFP-talin marker provides a reliable solution to circumvent the toxic effect of constitutive expression of F-actin interacting proteins, and the destructive effect of fixation techniques. We interpret the aforementioned data as the consequence of a specific degradation of F-actin arrays located at active growing sites in WT cells during the fixation process. Absence of tip growth in ADF-KO strains generates cells with a more uniform thick cell wall that protects cortical structures from degradation during fixation.

Noticeably, the position of these arrays in WT matched perfectly with the accumulation pattern of proteins ArpC4 [Perroud and Quatrano, 2006] and Brick1 [Perroud and Quatrano, 2008] at the growing tip of apical cells. Furthermore, the predicted hierarchical relation between Brick1 and ArpC4 was observed, since tip accumulation of Brick1 is normal in Arpc4-KO whereas Arc4 fail to accumulate in Brick1-KO [Perroud and Quatrano, 2008]. Taken together, these results are consistent with the concept that tip growth in *P. patens* protonemal cells is linked to the formation of an apical F-actin array that is involved in vesicle docking and delivery. Formation of the complex depends directly on the Arp2/3 complex which is activated through the Scar/Wave signaling pathway. In leafy shoots, which essentially develop by diffuse growth, Arp2/3 dependent formation of F-actin array would only contribute to establish localized growth domains similar to those involved in the formation of lobes in pavement cells of flowering plants.

A *brick1* mutant of *P. patens* differentiates normal stunted gametophores, but displays a more dramatic protonemal phenotype than *arp3* characterized by loss of the orientation of cell division. This suggests the involvement of the Scar/Wave complex in the activation of the Arp2/3 complex and of other F-actin structures that would be more directly involved in the establishment of cell polarity. The dramatic and almost lethal phenotype observed in PRF-KO and ADF-KD moss strains associated with defective tip growth and cell polarization clearly indicates that these proteins are essential for F-actin dynamics and preclude any further discussions on their specific function during moss development. Yet a hierarchical relation between these partners of actin dynamics can be outlined, with profilin and ADF acting as essential actors of the play, the Scar/Wave complex as intermediate between signaling molecules and local effectors, and the Arp2/3 complex as a direct activator of specific F-actin structures involved in localized cell expansion processes.

In the recent years major progress has been made in our understanding of the relation between actin dynamics and plant development. Subtle developmental phenotypes have been associated with mutations in the Scar/Wave - Arp2/3 signaling pathway in *Arabidopsis* [Deeks and Hussey, 2005, Mathur, 2005, 2006]. We identified in this study distinct F-actin structures that are specifically affected by loss of function of the

Arp2/3 complex in *P. patens*. Several studies suggest the presence of F-actin at the cap of plant tip growing cells such as root hair or pollen tubes, but the question remains controversial. Thus, existence of similar F-actin structures at localized cell expansion domains in model plant species deserves further experimental evidence to be confirmed. Several moss mutants affected in F-actin dynamics have been recently described and the regulating pathways look very similar in moss and model flowering plants. Comparative studies of actin dynamics in model plants and moss with its outstanding functional genomics and cell biology facilities will further increase our comprehension of the relation between plant development and the actin cytoskeleton.

REFERENCES

Ashton NW, Cove DJ. 1977. Isolation and preliminary characterization of auxotrophic and analog resistant mutants of moss. *Physcomitrella patens*. Mol Gen Genet 154(1):87–95.

Augustine RC, Vidali L, Kleinman KP, Bezanilla M. 2008. Actin depolymerizing factor is essential for viability in plants, and its phosphoregulation is important for tip growth. Plant J 54(5):863–875.

Balasubramanian MK, Feoktistova A, McCollum D, Gould KL. 1996. Fission yeast Sop2p: A novel and evolutionarily conserved protein that interacts with Arp3p and modulates profilin function. EMBO J 15(23):6426–6437.

Basu D, Le J, El-Essal SED, Huang S, Zhang CH, Mallery EL, Koliantz G, Staiger CJ, Szymanski DB. 2005. DISTORTED3/SCAR2 is a putative *Arabidopsis* WAVE complex subunit that activates the Arp2/3 complex and is required for epidermal morphogenesis. Plant Cell 17(2):502–524.

Bezanilla M, Pan A, Quatrano RS. 2003. RNA interference in the moss *Physcomitrella patens*. Plant Physiol 133(2):470–474.

Bezanilla M, Perroud PF, Pan A, Klueh P, Quatrano RS. 2005. An RNAi system in Physcomitrella patens with an internal marker for silencing allows for rapid identification of loss of function phenotypes. Plant Biol 7(3):251–257.

Chang F, Peter M. 2002. Cell biology - Formins set the record straight. Science 297(5581):531–532.

Christensen AH, Sharrock RA, Quail PH. 1992. Maize polyubiquitin genes - structure, thermal perturbation of expression and transcript splicing, and promoter activity following transfer to protoplasts by electroporation. Plant Mol Biol 18(4):675–689.

Cove D, Bezanilla M, Harries P, Quatrano R. 2006. Mosses as model systems for the study of metabolism and development. Annu Rev Plant Biol 57:497–520.

Deeks MJ, Hussey PJ. 2005. Arp2/3 and SCAR: Plants move to the fore. Nat Rev Mol Cell Bio 6(12):954–964.

Dos Remedios CG, Chhabra D, Kekic M, Dedova IV, Tsubakihara M, Berry DA, Nosworthy NJ. 2003. Actin binding proteins: Regulation of cytoskeletal microfilaments. Physiol Rev 83(2):433–473.

Finka A, Schaefer DG, Saidi Y, Goloubinoff P, Zryd JP. 2007. In vivo visualization of F-actin structures during the development of the moss *Physcomitrella patens*. New Phytol 174(1):63–76.

Girod PA, Fu HY, Zryd JP, Vierstra RD. 1999. Multiubiquitin chain binding subunit MCB1 (RPN10) of the 26S proteasome is essential for developmental progression in *Physcomitrella patens*.. Plant Cell 11(8):1457–1471.

Harborth J, Elbashir SM, Bechert K, Tuschl T, Weber K. 2001. Identification of essential genes in cultured mammalian cells using small interfering RNAs. J Cell Sci 114(24):4557–4565.

Harries PA, Pan AH, Quatrano RS. 2005. Actin-related protein2/3 complex component ARPC1 is required for proper cell morphogenesis and polarized cell growth in *Physcomitrella patens*. Plant Cell 17(8):2327–2339.

Hudson AM, Cooley L. 2002. A subset of dynamic actin rearrangements in *Drosophila* requires the Arp2/3 complex. J Cell Biol 156(4):677–687.

Imaizumi T, Kadota A, Hasebe M, Wada M. 2002. Cryptochrome light signals control development to suppress auxin sensitivity in the moss *Physcomitrella patens*. Plant Cell 14(2): 373–386.

Le J, Mallery EL, Zhang CH, Brankle S, Szymanski DB. 2006. Arabidopsis BRICK1/HSPC300 is an essential WAVE-complex subunit that selectively stabilizes the Arp2/3 activator SCAR2. Curr Biol 16(9):895–901.

Lees-Miller JP, Henry G, Helfman DM. 1992. Identification of Act2, an essential gene in the fission yeast *Schizosaccharomyces pombe* that encodes a protein related to actin. Proc Natl Acad Sci USA 89(1):80–83.

Mathur J. 2005. The ARP2/3 complex: Giving plant cells a leading edge. Bioessays 27(4):377–387.

Mathur J. 2006. Local interactions shape plant cells. Curr Opin Cell Biol 18:40–46.

Morrell JL, Morphew M, Gould KL. 1999. A mutant of Arp2p causes partial disassembly of the Arp2/3 complex and loss of cortical actin function in fission yeast. Mol Biol Cell 10(12):4201–4215.

Muller J, Menzel D, Samaj J. 2007. Cell-type-specific disruption and recovery of the cytoskeleton in *Arabidopsis thaliana* epidermal root cells upon heat shock stress. Protoplasma 230(3–4):231–242.

Perroud PF, Quatrano RS. 2006. The role of ARPC4 in tip growth and alignment of the polar axis in filaments of *Physcomitrella patens*. Cell Motil Cytoskeleton 63(3):162–171.

Perroud PF, Quatrano RS. 2008. BRICK1 Is required for apical cell growth in filaments of the moss *Physcomitrella patens* but not for gametophore morphology. Plant Cell 20(2):411–422.

Quader H, Schnepf E. 1989. Actin filament array during side branch initiation in protonema cells of the moss *Funaria hygrometrica* - an actin organizing center at the plasma-membrane. Protoplasma 151(2–3):167–170.

Rensing SA, Lang D, Zimmer AD, Terry A, Salamov A, Shapiro H, Nishiyama T, Perroud PF, Lindquist EA, Kamisugi Y, Tanahashi T, Sakakibara K, Fujita T, Oishi K, Shin-I T, Kuroki Y, Toyoda A, Suzuki Y, Hashimoto S, Yamaguchi K, Sugano S, Kohara Y, Fujiyama A, Anterola A, Aoki S, Ashton N, Barbazuk WB, Barker E, Bennetzen JL, Blankenship R, Cho SH, Dutcher SK, Estelle M, Fawcett JA, Gundlach H, Hanada K, Heyl A, Hicks KA, Hughes J, Lohr M, Mayer K, Melkozernov A, Murata T, Nelson DR, Pils B, Prigge M, Reiss B, Renner T, Rombauts S, Rushton PJ, Sanderfoot A, Schween G, Shiu SH, Stueber K, Theodoulou FL, Tu H, Van de Peer Y, Verrier PJ, Waters E, Wood A, Yang LX, Cove D, Cuming AC, Hasebe M, Lucas S, Mishler BD, Reski R, Grigoriev IV, Quatrano RS, Boore JL. 2008. The *Physcomitrella* genome reveals evolutionary insights into the conquest of land by plants. Science 319(5859):64–69.

Saidi Y, Finka A, Chakhporanian M, Zryd JP, Schaefer DG, Goloubinoff P. 2005. Controlled expression of recombinant proteins in *Physcomitrella patens* by a conditional heat-shock promoter: A tool for plant research and biotechnology. Plant Mol Biol 59(5):697–711.

Sambrook J, Fritsch EF, Maniatis T. 1989. Molecular Cloning: A Laboratory Manual. New York, NY: Cold Spring Harbor Press.

Sawa M, Suetsugu S, Sugimoto A, Miki H, Yamamoto M, Takenawa T. 2003. Essential role of the *C. elegans* Arp2/3 complex in cell migration during ventral enclosure. J Cell Sci 116(8): 1505–1518.

Schaefer DG. 2002. A newmoss genetics: Targeted mutagenesis in *Physcomitrella patens*. Annu Rev Plant Biol 53:477–501.

Schaefer DG, Zryd JP. 1997. Efficient gene targeting in the moss *Physcomitrella patens*. Plant J 11(6):1195–1206.

Szymanski DB. 2005. Breaking the WAVE complex: The point of *Arabidopsis trichomes*. Curr Opin Plant Biol 8(1):103–112.

Vidali L, Augustine RC, Kleinman KP, Bezanilla M. 2007. Profilin is essential for tip growth in the moss *Physcomitrella patens*. Plant Cell 19(11):3705–3722.

Winter D, Podtelejnikov AV, Mann M, Li R. 1997. The complex containing actin-related proteins Arp2 and Arp3 is required for the motility and integrity of yeast actin patches. Curr Biol 7(7):519–529.

Winter DC, Choe EY, Li R. 1999. Genetic dissection of the budding yeast Arp2/3 complex: A comparison of the in vivo and structural roles of individual subunits. Proc Natl Acad Sci USA 96(13):7288–7293.

Yae K, Keng VW, Koike M, Yusa K, Kouno M, Uno Y, Kondoh G, Gotow T, Uchiyama Y, Horie K, Takeda J. 2006. Sleeping beauty transposon-based phenotypic analysis of mice: Lack of Arpc3 results in defective trophoblast outgrowth. Mol Cell Biol 26(16):6185–6196.

Yoneda A, Kutsuna N, Higaki T, Oda Y, Sano T, Hasezawa S. 2007. Recent progress in living cell imaging of plant cytoskeleton and vacuole using fluorescent-protein transgenic lines and three-dimensional imaging. Protoplasma 230(3–4):129–139.

Zallen JA, Cohen Y, Hudson AM, Cooley L, Wieschaus E, Schejter ED. 2002. SCAR is a primary regulator of Arp2/3-dependent morphological events in *Drosophila*. J Cell Biol 156(4):689–701.